# Optical observations of type IIP supernova 2004dj: Evidence for the asymmetry of $^{56}$ Ni ejecta

N.N. Chugai $^1,$ S.N. Fabrika $^2,$ O.N. Sholukhova $^2,$ V.P. Goranskij $^2,$  P.K. Abolmasov $^3,$  and V.V. Vlasyuk $^2$ 

<sup>1</sup>Institute of astronomy RAS, Moscow

 $^2 Special\ astrophysical\ observatory,\ Zelenchuk$ 

 $^3 Sternberg\ astronomical\ institute,\ Moscow$ 

## **ABSTRACT**

The photometric and spectroscopic observations of nearby type IIP supernova 2004dj are presented. The  $^{56}$ Ni mass estimated from the light curve is  $\approx 0.02~M_{\odot}$ . This estimate is found to be consistent with the H $\alpha$  luminosity. SN2004dj reveals a strong asymmetry of the H $\alpha$  emission line at the nebular epoch with the shift of the maximum of  $-1600~{\rm km~s^{-1}}$ . A similar asymmetric component is detected in H $\beta$ , [O I] and [Ca II] lines. The line asymmetry is interpreted as a result of the asymmetry of  $^{56}$ Ni ejecta. The H $\alpha$  profile and its evolution are reproduced in the model of the asymmetric bipolar  $^{56}$ Ni and spherical hydrogen distributions. The mass of the front  $^{56}$ Ni jet is comparable to the central component and twice as larger compared to the rear  $^{56}$ Ni jet. We note that the asymmetric bipolar structure of of  $^{56}$ Ni ejecta is revealed also by SN1999em, another type IIP supernova.

## 1. Introduction

Supernova SN2004dj is discovered on 2004 July 31 in Sc galaxy NGC2403 (Nakano et al. 2004). According to spectra and light curve (Korcakova 2005) this is a usual type IIP supernova (i.e., with plateau in the light curve) detected in 30-45 days after the explosion. With the distance of 3.13 Mpc (Freedman et al. 2001) this is closest SNIIP after SN1987A. Given the peculiar nature of the latter SN2004dj turns out to be closest ever normal SNIIP observed.

Type IIP supernovae are related with the explosion of a massive  $(10 - 25 M_{\odot})$  red supergiant following the collapse of iron core. Three versions of the explosion mechanism

have been proposed: (1) neutrino mechanism (Colgate & White 1966; Buras et al. 2003); (2) magneto-rotational mechanism (Ardelyan et al. 2005); (3) rotational fragmentation of a new-born neutron star with the subsequent explosion of low-mass ( $\sim 0.1~M_{\odot}$ ) fragment (Blinnikov et al. 1990). Whatever happens the subsequent shock wave ejects the envelope with the sufficient internal energy to provide the SNIIP luminosity at the plateau stage (Grasberg et al. 1971). The shock wave propagation in the silicon mantle results in the synthesis of radioactive <sup>56</sup>Ni; its decay via <sup>56</sup>Ni–<sup>56</sup>Co–<sup>56</sup>Fe maintains the SNIIP luminosity at the tail of the light curve (Weaver & Woosley 1980). Neither of proposed explosion mechanism is able as yet to reproduce empirical values of the explosion energy and ejected <sup>56</sup>Ni mass of SNIIP.

The proximity of SN2005dj provides us an opportunity to study in greater details the observational display of an explosion of normal SNIIP. Unfortunately, supernova was discovered long after the outburst so the explosion energy cannot be recovered from a hydro modeling. Yet the light curve and H $\alpha$  luminosity at the nebular epoch can provide us an estimate of the <sup>56</sup>Ni mass, another vital property of the explosion mechanism.

Of particular interest would be the emission line profiles at the nebular epoch, which could provide us valuable information about the possible explosion asymmetry in SNIIP. The asymmetry issue emerged after the detection of the emission lines redshift in SN1987A (Phillips & Williams 1991) followed by the interpretation of this redshift as an effect of <sup>56</sup>Ni ejecta asymmetry (Chugai 1991). A similar phenomenon was recovered recently in the type IIP supernova SN1999em (Elmhamdi et al. 2003a). Herant et al. (1992) conjecture that the <sup>56</sup>Ni asymmetry as well as high pulsar velocities may be related to the violation of a point symmetry in core-collapse supernovae owing to the large scale neutrino convection.

Below we present results of spectral and photometric observations of SN2004dj in Special astrophysical observatory (SAO) at Zelenchuk. Apart from a qualitative analysis of the observational data we present estimates of  $^{56}$ Ni mass in SN2004dj from the light curve and the H $\alpha$  luminosity. The observed spectra reveal unusually strong asymmetry of the H $\alpha$  emission line. Given the importance of this phenomenon we concentrate on the study of the line asymmetry and its relationship with the asymmetry of  $^{56}$ Ni ejecta.

Henceforth we use the distance D = 3.13 Mpc (distance module  $\mu = 27.48$ ) according to cepheids (Freedman et al. 2001) and the redshift of 129 km s<sup>-1</sup> according to LEDA database.

### 2. Observations

Broad band BVRc photometry of SN2004dj was carried out at 1-m Zeiss telescope of SAO using CCD Electronika K-585 and EEV 42-40. The photometry data were also obtained at 60-cm telescope of Crimean station of SAI with CCD VersArray. These three detectors are shortened as K, E, and VA respectively. A local photometric standard around supernova is based on the UBVR standard in the vicinity of NGC 2403 (Zickgraf et al. 1990). The reduction of CCD images is made with the WinFITS package (V.P. Goranskij) using a method of corrected aperture measurements that permits us to deal with the inhomogeneous background in the vicinity of supernova. The accuracy of the photometric data is 0.005–0.01 mag. The data are presented in Table 1. The columns in order are Julian dates, magnitudes and the detector type. The first line of the Table 1 contains the photometry data on 2001 January 19, long before the explosion. We believe that these magnitudes refer to the star cluster S96 on which SN2004dj is superimposed.

The log of spectral observations which includes observation moments, spectrograph type, spectral range and resolution is presented in Table 2. Eight spectra were taken between 2004 October 18 and 2005 June 9. The first spectrum is obtained at the transition between the plateau and tail, whereas the rest ones were taken at the light curve tail. Three types of spectrograph were used in observations: (i) Scorpio, the universal focal reducer (Afanasiev & Moiseev 2005) of 6-m large azimuthal telescope (LAT), multi-pupil fiber spectrograph (MPFS) of LAT, and UAGS spectrograph of 1-m telescope of SAO. CCD images of spectra taken at Scorpio and UAGS are reduced using MIDAS package with the usual procedures of the extraction of cosmic rays, field flattening, and spectra extraction. The reduction of spectra taken at MPFS is performed using package written by V.L. Afanasiev, A.V. Moiseev and P.K. Abolmasov. In two cases (spectra No. 2 and 6 in Table 2) the atmospheric dispersion strongly modifies the spectral energy distribution. These spectra will not be used for the H $\alpha$  flux measurements, although they may well be used for the line profile analysis.

# 3. Photometry and <sup>56</sup>Ni mass

The V light curve according to our data and other available data<sup>1</sup> is plotted in Fig. 1. The time is counted from the adopted explosion moment JD2453170 (i.e., 2004 June 13). This choice is based upon the assumption that light curves of SN2004dj and SN1999gi, standard SNIIP (Leonard et al. 2002), are similar. This assumption is supported by the fact that the

<sup>&</sup>lt;sup>1</sup>http://www.astrosurf.com/snweb2/2004dj/Meas.htm

same fitting curve describes both sets of data reasonably well (Fig. 1). The approximation suggests the exponential behavior of the flux in V band at the tail  $F(V) \propto \exp(-t/111.26 \,\mathrm{d})$  in accordance with the radioactive decay of  $^{56}\mathrm{Co}^{-56}\mathrm{Fe}$ .

The two last measurements (day 266 and 267) show excess  $\approx 0.17$  mag over the exponential behavior (Fig. 1). Most of this excess is likely related to the contribution of the star cluster S96. Given the pre-explosion magnitude (Table 1) we find that the star cluster on day 266.5 must contribute 0.14 mag assuming exponential behavior of the intrinsic V magnitude of SN2004dj. The light of S96, indeed, accounts for, practically, all the excess.

Galactic reddening towards NGC2403 is E(B-V)=0.062 (Schlegel et al. 1998). This value is adopted as a total reddening of supernova in our and host galaxy. With this reddening the intrinsic B-V color of SN2004dj according to our and other available data (see previous footnote) is displayed in Fig. 2. We plotted also the SN1987A color (Catchpole et al. 1987, 1988) and the lower envelope of intrinsic colors of SNIIP (Elmhamdi et al. 2003b). The B-V color of SN2004dj coincides wih the lower envelope of SNIIP colors, which indicates that the adopted reddening is close to the actual value. On the other hand Wang et al. (2005) upon the basis of the population synthesis of the star cluster S96 derive the reddening  $E(B-V) \sim 0.35$ . The contradiction may be resolved if the light form S96 is absorbed in the cool shell around this cluster, while the supernova resides outside the shell, closer to the observer.

The V-R color of SN2004dj (Fig. 2, inset) around day 150 is by 0.3 mag lower than that of SN1987A. However, the color difference gets smaller with time and disappears around day 200. This indicates that the spectral energy distributions (SED) for both supernova in the long wavelength range ( $\lambda > 5000 \text{ Å}$ ) at  $t \geq 200 \text{ d}$  are similar. This fact is of importance for the photometric estimate of <sup>56</sup>Ni mass in SN2004dj.

The amount of  $^{56}$ Ni in the envelope can be found from a comparison of  $M_V$  absolute magnitudes of SN2004dj and SN1987A at the early nebular epoch (t < 250 d) when the envelope is optically thick for gamma-rays, so one may adopt that all the radioactive luminosity is instantly re-emitted in the optical. The method assumes that the distance and reddening are well known and the bolometric correction is similar for both supernovae. The latter seems to disagree with the apparent difference of their B-V colors. However, one should keep in mind that at this epoch the bulk of the energy is emitted in the long wavelength range ( $\lambda > 5000$  Å), in which SED are similar around and after day 200 as indicated by the their V-R colors (Fig. 2). Therefore, using SN1987A as a template we hopefully can recover the amount of  $^{56}$ N in SN2004dj from V magnitude around day 200.

Using the exponential approximation of the V light curve of SN2004dj (Fig. 1) we get

V=15.32 on day 200. With the reddening E(B-V)=0.062 and standard extinction law (Seaton 1979) the absorption is  $A_V=0.19$ . With the distance module  $\mu=27.48$  for NGC2403 one gets  $M_V=-14.01$  on day 200. On the other hand, for SN1987A at this epoch V=5.09 (Catchpole et al. 1988). Adopting the distance 50 kpc and absorption  $A_V=0.6$  one gets  $M_V=-14.01$  on day 200. Thus on day 200 SN1987A is brighter in V band compared to SN2004dj by 1.53 mag. With the <sup>56</sup>Ni mass 0.075  $M_{\odot}$  in the SN1987A envelope (Suntzeff & Bouchet 1991) we conclude that the amount of <sup>56</sup>Ni in SN2004dj is  $M(^{56}\text{Ni}) \approx 0.02 \ M_{\odot}$ .

The uncertainty of the  $^{56}$ Ni mass related to the error in distance (Freedman et al. 2001) is of 20%. The uncertainty related with the extinction unlikely exceeds 10% taking into account low reddening indicated by the extremely "blue" color B-V of SN2004dj. Some contribution to the error of  $^{56}$ Ni mass may be related to the possible difference of bolometric corrections of SN2004dj and SN1987A. To summarize, the total error of the  $^{56}$ Ni mass estimate is  $\sim 30\%$ .

Independently, the  $^{56}$ Ni mass may be estimated using the empirical relation between amount of  $^{56}$ Ni and parameter S = dV/dt that characterizes the steepness of the V light curve at the transition between plateau and tail (Elmhamdi et al. 2003b). In the case of SN2004dj we find  $S = 0.17 \pm 0.04$  mag. day<sup>-1</sup>. Using the empirical relation from (Elmhamdi et al. 2003b) one gets  $M(^{56}$ Ni) =  $0.013 \pm 0.004$   $M_{\odot}$  that is consistent within errors with the estimate found above.

#### 4. Spectrum and its evolution

## 4.1. Qualitative analysis

The observed spectra of SN2004dj are presented in Fig. 3. The last two spectra (Table 2) are merged into the single spectrum since at this epoch the spectral evolution is slow. The appearance and evolution of SN2004dj spectrum are similar to those of ordinary SNIIP at the nebular epoch. The late time spectrum is dominated by emission lines of H $\alpha$ , [O I] 6300, 6364 Å and [Ca II] 7291, 7324 Å on the background of the relatively weak quasicontinuum. According to general wisdom, the latter is composed by the emission of numerous metal lines, mostly Fe II, that originates as a result of the absorption of ultraviolet photons generated in central parts of the envelope due to the reprocessing of the radioactive luminosity (Xu & McCray 1991). The scattering and absorption of the quasicontinuum in metal and hydrogen lines in outer layers produces broad P Cygni profiles, e.g., H $\beta$ , Fe II lines of the multiplet 42, Na I doublet (Fig. 3).

A spectacular feature of the SN2004dj spectra, never observed before in SNIIP, is the strong blueshift of emission line maxima, most apparent in H $\alpha$  (Fig. 4). The profile of this line is clearly asymmetric with the maximum at  $-1600 \text{ km s}^{-1}$  in early (127 and 131 days) spectra. The blueshift decreases with time down to -600 km s<sup>-1</sup> on day 330. The blue peak, although weaker, is present also in H $\beta$ . Remarkably, on day 131 the H $\alpha$  profile shows double horn structure with the red horn shift of  $\approx 1600 \text{ km s}^{-1}$ . This indicates the bipolar, although asymmetric, structure of the hydrogen excitation.

Among type IIP supernovae only two cases of significant H $\alpha$  line asymmetry were mentioned earlier: SN1987A (Phillips & Williams 1991) and SN1999em (Elmhamdi et al. 2003a). In both cases the redshift was reported. The redshift in SN1987A has been interpreted as a result of the ejection of significant amount of  $^{56}$ Ni in the far hemisphere in otherwise spherical envelope (Chugai 1991). The similar interpretation was proposed for the redshift of H $\alpha$  and HeI 10830 Å lines in SN1999em (Elmhamdi et al. 2003a). We adopt the same explanation for the H $\alpha$  asymmetry in SN2004dj with the only difference that in this case the  $^{56}$ Ni distribution is skewed towards the observer.

The manifestation of the line asymmetry in SNIIP is displayed in Fig. 5, which shows H $\alpha$  and [Ca II] doublet in SN2004dj on day 149, SN1987A on day 198 (Phillips & Williams 1991) and SN1999em on day 140 (Elmhamdi et al. 2003a). Apart from the sign of asymmetry, SN2004dj differ by the larger shift and the amplitude of the asymmetric H $\alpha$  component. The [Ca II] doublet of SN2004dj differs also very much from that in other supernovae (Fig. 5). SN2004dj shows the striking blue peak in [Ca II] at  $-1600 \text{ km s}^{-1}$  that is seen in H $\alpha$ . This peak reflects, presumably, the local overexcitation of Ca II related to the asymmetry of <sup>56</sup>Ni ejecta likewise in H $\alpha$ .

Other spectral differences between SN2004dj and SN1999em related to different signs of asymmetry are noteworthy. The absorption component of H $\alpha$  in SN2004dj is markedly weaker than in SN1999em (Fig. 6). This is caused by the presence of the blue emission peak in SN2004dj that fills in the absorption. Absorption component of H $\beta$ , on the contrary, is stronger in SN2004dj. The reason for that is also the ejection of <sup>56</sup>Ni primarily towards the observer. This causes higher hydrogen excitation in the near hemisphere of SN2004dj compared to SN1999em where most of <sup>56</sup>Ni is shifted towards the far hemisphere. As a result the H $\beta$  optical depth in the near hemisphere of SN2004dj is greater than in SN1999em.

Interestingly, spectra of SN2004dj at the plateau epoch (Korcakova et al. 2005) demonstrate larger expansion velocities of the H $\alpha$  absorption minimum compared to SN1999em. On JD2453221 (day 51 for the assumed outburst date) radial velocity of the H $\alpha$  absorption minimum is -6955 km s<sup>-1</sup> (Korcakova et al. 2005) compared to -5000 km s<sup>-1</sup> in SN1999em on 54 day (Elmhamdi et al. 2003a). We believe that higher velocity of SN2004dj reflects

the higher degree of the hydrogen excitation in the near hemisphere rather then higher energy-to-mass ratio.

Another remarkable peculiarity of SN2004dj is the quasicontinuum shape in the range of 5000–5700 Å which differ from that in SN1999em. Note, the quasicontinua of SN1999em and SN1987A are rather similar in the same range. The plausible explanation involves the different sign of <sup>56</sup>Ni asymmetry in SN2004dj and SN1999em. Actually, the <sup>56</sup>Ni displacement should result in the different conditions for the quasicontinua formation in asymmetric hemispheres because of the different excitation degree.

# 4.2. H $\alpha$ luminosity and <sup>56</sup>Ni mass

The integrated H $\alpha$  flux is measured in the spectra which were calibrated using V and Rc photometric data. The resulting H $\alpha$  flux is the average between fluxes derived from V and Rc calibrations. We omit spectra on days 131 and 237 which are strongly affected by the atmospheric dispersion, and the spectrum on day 330 which cannot be calibrated confidently because the strong [Ca II] emission is missing. The obtained H $\alpha$  fluxes, uncorrected (F) and corrected ( $F^{corr}$ ) for the dust absorption, are given in Table 3. The last column is the H $\alpha$  luminosity. The error of the flux (0.12 dex) is estimated as half of the maximal difference of fluxes derived from V and Rc calibrations.

The H $\alpha$  luminosity at the nebular epoch is used here to estimate  $^{56}$ Ni in SN2004dj likewise this was done earlier for SNIIP (Elmhamdi et al. 2003b). The method suggests the computation of H $\alpha$  luminosity powered by the radioactive decay  $^{56}$ Co –  $^{56}$ Fe. Three levels plus continuum hydrogen atom is adopted, although recombinations on the excited levels are included. The photoionization from the second and third level by continua is taken into account. Radiation transfer in continua is treated in the escape probability approximation (Chugai 1987). The two-zone model envelope consists of the macroscopically mixed core and outer envelope. The model parameters are the mass M, kinetic energy E,  $^{56}$ Ni mass, mass fraction in the core  $f_{\rm mix}$  and the fraction of the core residing in metals and helium  $f_{\rm m}$ . The quasicontinuum SED is described by the plankian spectrum with the color temperature  $T_{\rm c}$ . In contrast to the previous version here the electron temperature  $T_{\rm e}$  is calculated from the energy balance which takes into account cooling in Ca II, Mg II, Fe II (approximately), O I lines, ff-emission and adiabatic cooling. We abandon the approximation of the homogeneous density assuming that the density in the core is three times larger than the outer shell density. This mimics the density distribution in the real SNIIP envelope.

The model takes into account the outcome of the macroscopic mixing of <sup>56</sup>Ni in the

exploding star with the stratified chemical composition. We adopt that fragments of the  $^{56}$ Ni material are embedded in cocoons composed of metals and helium, i.e., of the material lacking the hydrogen. The optical depth of the cocoon for gamma-rays is determined by the mass and the surface area of cocoons,  $\tau_{\rm c} = k f_{\rm m} f_{\rm mix} M/(4\pi f_{\rm s} R_1^2)$ , where k = 0.03(1+X) cm<sup>2</sup> g<sup>-1</sup> (Fransson and Chevalier 1989), X is the hydrogen abundance,  $R_1$  is the radius of the mixed core,  $f_{\rm s}$  is the mixing parameter. The latter is the ratio of the cocoon surface area to  $4\pi R_1^2$ . Below we show results for  $f_{\rm s} = 2$  (moderate mixing) and  $f_{\rm s} = 20$  (strong mixing). The adopted ejecta mass is  $M = 13~M_{\odot}$ , presumably the mass of SN1999em ejecta (Nadyozhin 2003) that corresponds to the 15  $M_{\odot}$  main sequence mass. The kinetic energy is  $E = 10^{51}$  erg, the typical value for SNIIP (Nadyozhin 2003). Other parameters are  $f_{\rm mix} = 0.4$ ,  $f_{\rm m} = 0.3$ , i.e.,  $\approx 1.56~M_{\odot}$  of the core resides in metals and helium. The remainder of helium, from several tens to  $\sim 1~M_{\odot}$  is presumably mixed with the hydrogen. Note, for the star with the initial mass  $M \approx 15~M_{\odot}$  the predicted mass of newly synthesised metals and helium in the supernova is about 3  $M_{\odot}$  (Woosley & Weaver 1995), in agreement with our assumptions.

The optimal models of the H $\alpha$  luminosity in SN1999em at the nebular epoch  $t \geq 130$  days are presented in Fig. 7 for the two values of the mixing parameter  $f_{\rm s}$ . The adopted  $^{56}{\rm Ni}$  mass  $M(^{56}{\rm Ni})=0.027~M_{\odot}$  is equal to the value recovered from the tail of V light curve (Elmhamdi et al. 2003b). The color temperature of the quasicontinuum is the only free parameter. Its value turns out to be  $T_{\rm c}=5500~{\rm K}$  for the model with  $f_{\rm s}=2$  and  $T_{\rm c}=5000~{\rm K}$  for  $f_{\rm s}=20$ .

For SN2004dj we adopt the same model as for SN1999em. The only difference is the  $^{56}$ Ni mass, which is  $M(^{56}$ Ni) = 0.02  $M_{\odot}$ , the value recovered from the V light curve. The plot (Fig. 7, lower panel) shows that the model of the H $\alpha$  luminosity with this amount of  $^{56}$ Ni fits to the observational data within errors. Of course, this fact cannot be considered as a proof that the  $^{56}$ Ni mass is actually  $\approx 0.02~M_{\odot}$  given uncertainties of other parameters. On the other hand, this indicates that the  $^{56}$ Ni mass recovered from the V light curve is approximately consistent with the H $\alpha$  luminosity.

# 5. Line asymmetry and $^{56}$ Ni distribution

The line profile formed in the supernova envelope with the kinematic of the homologous expansion (v = r/t) depends on the distribution of the level populations and the continuum optical depth. At the nebular epoch the absorption in the quasicontinuum is weak in the red part of the spectrum ( $\lambda > 5000$  Å). The profile of emission lines of H $\alpha$ , [O I] 6300, 6364 Å and [Ca II] 7291, 7324 Å thus contain the information about the asymmetry of the radiation

sources throughout the envelope including deep central zone.

# 5.1. [O I] 6300, 6364 Å lines

The lines in [O I] and [Ca II] doublets are partially superimposed, so it would be reasonable to recover true line profile using representation of each line as a superposition of the minimal number of gaussian components. Each gaussian component is characterized by its radial velocity  $v_r$ , Doppler width w and relative amplitude A.

Oxygen doublet [O I] 6300, 6364 Å is a convenient case for the decomposition because the velocity interval between lines is large (3000 km s<sup>-1</sup>). Using only two gaussian components, central and blueshifted, we are able to reproduce successfully the doublet profile on day 237 and 330 (Fig. 8). Parameters of components (displacement, width, amplitude) are given in Table 4). The line profiles of [O I] and H $\alpha$  on day 237 are quite similar (Fig. 4); on day 330, however, the difference is remarkable: the [O I] maximum is at zero, while the H $\alpha$  maximum is blueshifted at  $\approx -700$  km s<sup>-1</sup>. This fact reflects, probably, the different distribution of hydrogen and oxygen.

The increasing role of the central component can be explained in a picture of the two  $^{56}$ Ni components. Let the central component be embedded into the cocoon that is optically thick for gamma-rays and does not contribute in the [O I] doublet emission. Note, the cocoon material may be even composed by oxygen and yet be unseen in [O I] lines. This is the case, if formed CO and/or SiO molecules cools the oxygen material (Liu & Dalgarno 1995). As the envelope expands, the cocoon gets optically thin and gamma-rays efficiently excite outer oxygen material thus increasing the role of the central component. A similar effect in  $H\alpha$  will be studied below (Section 5.3).

For the doublet decomposition we used some value of the doublet ratio R = I(6300)/I(6364). The latter is equal to the ratio of line specific luminosities  $h\nu_{ik}n_kA_{ki}\beta_{ik}$  [erg s<sup>-1</sup> cm<sup>-3</sup>], where  $\beta_{ik}$  is the escape probability, while the other notations are obvious. The optimal R values (Table 4, last column) are lower than nebular one, R = 3, which implies that [O I] lines are optically thick. The similar situation takes place in other SNIIP (Spyromilio & Pinto 1991; Chugai 1988). The doublet ratio is determined primarily by the oxygen concentration and only weakly depends on the electron temperature, since the excitation potential of the lower level of the transition of 6364 Å is only 0.02 eV. Since the oxygen is mostly neutral the ratio R permits us to recover the oxygen density in the line forming zone. The observed ratio R = 1.33 on day 237 leads to the oxygen number density  $n(O) = 6.63 \times 10^9 (237 \, d/t)^3 \, cm^{-3}$ , where t in days and t0 is adopted. The density evolution t0 is t1 predicts

the ratio R=1.77 on day 330, in good agreement with the value R=1.8 found from observations (Table 4). This confirms the adopted explosion date of SN2004dj, although the accuracy of the reconstruction of the explosion date from the ratio R is not better than  $\pm 30$  days.

## 5.2. [Ca II] 7391, 7324 Å lines

The lines of [Ca II] doublet also can be represented by two gaussian components, central and blueshifted (Fig. 9, Table 5). However, the broad central component shows some deviation from gaussian shape and requires an additional weak narrow component (Fig. 9, inset). On day 237 when [Ca II] and [O I] doublets can be compared, the line profiles are roughly similar, although some differences are apparent. Particularly, the blue component of [Ca II] shows the same shift but 1.6 times more narrow. The central component, on the contrary, is 1.7 times broader than in [O I] case. The average radial velocity of [Ca II] line (e.g., 7291 Å) is -150 km s<sup>-1</sup> on day 237, i.e., lower than that of [O I] line at the same epoch (-770 km s<sup>-1</sup>).

These differences are likely caused by the formation of these lines in different zones. Actually, stellar evolution for massive stars (e.g.,  $15~M_{\odot}$ ) and supernova models predicts that Ca is synthesised in two processes: static oxygen burning in the presupernova and explosive oxygen burning during the shock wave propagation (Woosley & Weaver 1995). Calcium, therefore, is expected to reside in products of the oxygen burning (in Si/S matter), not in the oxygen matter. Moreover, the [Ca II] 7391, 7324 Å lines may also form in hydrogen or helium material (Li & McCray 1993) with the main sequence abundance.

Given uncertainty of the site of the [Ca II] doublet formation, it is interesting that the doublet ratio on day 149 is  $R = I(7291)/I(7324) \approx 1.1$ , i.e., lower than the nebular one (R=1.5). If this is caused by the optical depth effect, then the required number density of Ca should be  $n(\text{Ca}) > 3.6 \times 10^6 (149 \, \text{d/t})^3 \, \text{cm}^{-3}$ . Assuming that the [Ca II] doublet is emitted by the hydrogen matter we find the required density of hydrogen for normal Ca abundance  $\rho > 3.7 \times 10^{-12} (149 \, \text{d/t})^3 \, \text{g cm}^{-3}$ . This should be compared with the oxygen density found from oxygen doublet ratio,  $\rho \approx 7 \times 10^{-13} (149 \, \text{d/t})^3 \, \text{g cm}^{-3}$ . The latter turns out to be five time lower compared to the required hydrogen density, quite reverse to expectations. Actually, the analysis of SN1987A shows that the oxygen is distributed in dense condensations with the filling factor of  $f \sim 0.1$  and the oxygen density is by order of magnitude greater than the average density (Spyromilio & Pinto 1991; Chugai 1988). The found controversy indicates that the hypothesis of the [Ca II] doublet formation in the hydrogen material faces serious problems. However, given uncertainty of the quasicontinuum behavior in the 7300 Å band

one cannot preclude that we underestimated the doublet ratio. We thus do not rule out the formation of [Ca II] doublet in the hydrogen material although this possibility seems doubtful.

## 5.3. Modeling $H\alpha$ asymmetry

Here we address the H $\alpha$  line profile and its connection with the asymmetry of the <sup>56</sup>Ni distribution. We facilitate the physics of the energy cascade resulting in the H $\alpha$  emission and assume that the specific H $\alpha$  luminosity,  $\eta = h\nu_{23}n_3A_{32}\beta_{23}$ , is proportional to the local deposition rate  $\eta = C\epsilon_{\rm d}$  with the constant factor C. To obtain the H $\alpha$  line profile one has to define the <sup>56</sup>Ni distribution and to calculate the distribution of the deposition  $\epsilon_{\rm d}$ . The gamma-ray transfer is computed in a single flight approximation with the absorption coefficient adopted above (section 4.2).

The model envelope expands homologously (v = r/t) and has the spherical mass distribution (but <sup>56</sup>Ni). The density is described by the exponential distribution  $\rho = \rho_0 \exp(-v/v_0)$  with  $\rho_0 \propto t^{-3}$ . The exponential law is fairly good for the bulk of the inner envelope where the power index  $|d \ln \rho/d \ln v|$  gradually increases outwards (e.g., Utrobin 2004). The parameters  $\rho_0$  and  $v_0$  are determined by M and E. We adopt as above  $M = 13 M_{\odot}$  and  $E = 10^{51}$  erg.

The <sup>56</sup>Ni distribution is set by three components: central homogeneous sphere and two cylindrical jets with the angle  $\theta$  between the jet axis and the line of sight (Fig. 10). In the regions, where jets are superimposed on the central spherical component, the density is assumed to be equal to the jet density. We found that the opposite condition is less consistent with observations. The density of <sup>56</sup>Ni in jets is assumed to decrease linearly outwards down to zero at the outer jet boundary. The chemical composition of the envelope is homogeneous with the hydrogen abundance X = 0.7. In the central zone of the radius  $R_s = v_s t$  the matter distribution is presumably inhomogeneous with the filling factor of the hydrogen matter linearly decreasing inwards from unity at  $R_s$  to zero in the center. This assumption is consistent with intuitive picture of the mixing of helium and metals with the hydrogen envelope.

The study of the parameter space of the model led us to conclude that only the version with cocoons around  $^{56}$ Ni material is able to reproduce the evolution of H $\alpha$  profile. The cocoon model has been already used above to describe the evolution of H $\alpha$  luminosity. Here this model should be refined given more complicated geometry of mixing. We assume that  $^{56}$ Ni is represented by an ensemble of spherical fragments each coated by cocoon of the optical depth  $\tau_c$  for gamma-rays. The average gamma-ray emissivity is then multiplied by

the attenuation factor  $\exp(-\tau_c)$ . We adopt  $\tau_c = const$  in the central zone of the radius  $R_s$ , while in jets outside the central zone, the cocoon optical depth decreases with the velocity v as

$$\tau_{\rm c} = \tau_0 \left( \frac{v_k - v}{v_k - v_{\rm s}} \right)^p \,, \tag{1}$$

where  $v_k$  is the outer velocity k-th jet (k = 1, 2). The adopted power index is p = 3. The parameter  $\tau_0$  may be written via the cocoon mass of  $M_c$  as  $\tau_0 = kM_c/4\pi f_s R_s^2$  where  $f_s$  is the mixing parameter introduced earlier (Section 4.2). The decrease of  $\tau_c$  outwards corresponds to the increase of the mixing degree. This is just what is expected from the mixing physics: the material propagated through the larger mass should experience larger mixing degree.

Parameters of the optimal model, i.e., the angle  $\theta$  between the line of sight and the axis of <sup>56</sup>Ni, the expansion velocity of the central component  $v_{\rm s}$ , boundary velocity of jets ( $v_{\rm 1}$ , and  $v_{\rm 2}$ ), the mass of jets, and cocoon mass for the mixing parameter  $f_{\rm s}=2$  are given in Table 5. The accuracy of the determination of velocities is about 20%, angle  $\theta$  is determined with the accuracy of 10°. Interestingly, while the model of the H $\alpha$  luminosity does not impose strict constraints on  $f_{\rm s}$ , we find that assuming a cocoon mass  $M_{\rm c} \sim 1~M_{\odot}$  requires a moderate mixing,  $f_{\rm s} \sim 2$ .

Model profiles of  $H\alpha$  with and without cocoon are plotted along with observations in Fig. 11. The model with cocoon is apparently more adequately describes profile and its evolution during 131–330 days. Note, within the same model we are able to describe the non-trivial change from asymmetric two-horn profile on day 131, through the plateau plus blue peak on day 149, towards smooth asymmetric profile with the blueshifted maximum.

The specific features of the recovered <sup>56</sup>Ni distribution are the bipolar structure and the deviation from the point symmetry. The mass of the front <sup>56</sup>Ni jet is comparable to the central component and twice as larger compared to the rear <sup>56</sup>Ni jet (Table 5). Note, there is no need to admit the asymmetry of hydrogen distribution, which otherwise would require extremely large degree of the supernova asymmetry.

The one-dimension projection of the recovered <sup>56</sup>Ni distribution on the line of sight and the jet axis are shown in Fig. 12. For comparison we show also the recovered line profile of [Ca II] 7291 Å on day 149 (Fig. 9), when the gamma-ray transfer effect is small and, therefore, the sources in [Ca II] lines follow the distribution of <sup>56</sup>Ni. While there is a general correspondence between [Ca II] line profile and <sup>56</sup>Ni distribution we see apparent differences. The <sup>56</sup>Ni projection on the line of sight does not show strong central peak that is present in [Ca II] line. This disparity indicates that the Ca distribution deviates from <sup>56</sup>Ni distribution.

Interestingly, we found that the major mass of <sup>56</sup>Ni should be isolated from the hydrogen by the cocoon that does not contain any hydrogen. Moreover, the mixing degree that

determine the the thickness of cocoon should not be large. The similar property of the  $^{56}$ Ni distribution has been revealed by Liu & Dalgarno (1995) in SN 1987A. To account for the evolution of CO 2.3 mcm emission they introduced a variable reduction factor for gammarays that decreases with time. This factor, we believe, reflects the existence of cocoons around  $^{56}$ Ni fragments in SN1987A as well.

## 6. Discussion and conclusion

We have presented results of the photometry and spectroscopy of SN2004dj, the usual type IIP supernova. We have estimated  $^{56}$ Ni mass from the comparison of light curves of SN2004dj and SN1987A and from the modeling of H $\alpha$  luminosity. Both estimates suggests the  $^{56}$ Ni mass of  $\approx 0.02~M_{\odot}$ . This is 3.8 times less than in SN1987A and comparable with  $^{56}$ Ni mass in SN1999em (0.02 – 0.027  $M_{\odot}$ , Elmhamdi et al. 2003a, 2003b).

The principal result of spectroscopic study of SN2004dj is the detection of a strong blueshift of the H $\alpha$  line that is interpreted as a result of the asymmetric ejection of  $^{56}$ Ni in the spherically-symmetric envelope. The modeling of the H $\alpha$  line profile led us to conclude that the structure of the profile and its evolution are well reproduced in the model of the asymmetric bipolar  $^{56}$ Ni ejecta with the two-fold difference of jet masses and the comparable masses of the massive jet and the central component.

We have found signatures of the bipolar structure in H $\alpha$  and [Ca II] line of SN1999em, which indicate that the asymmetric bipolar <sup>56</sup>Ni ejecta is not exception for SNIIP. Although in SN1987A spectral signatures of the bipolar structure are absent, Wang et al. (2002) see bipolar structure of inner region of SN1987A in images taken by HST. The detection of bipolar structure of <sup>56</sup>Ni ejecta at least in two normal SNIIP implies that bipolar explosion of the core-collapse supernovae can occure for a moderately rotating red supergiant core.

The significant deviation from the point symmetry in the <sup>56</sup>Ni distribution revealed by at least three supernovae, namely SN1987A, SN1999em and SN2004dj, suggests that the total momentum may be essentially non-zero for synthesised iron-peak ejecta in SNIIP. In this case the finite momentum is presumably compensated by the envelope or/and neutron star. According to recent study of proper motions of pulsars (Hobbs et al. 2005) neutron stars at birth acquire high velocities about 400 km s<sup>-1</sup> in average. These velocities unlikely could be explained by the sling effect of supernova in close binary, so the kick is the preferred explanation. The asymmetry of <sup>56</sup>Ni ejecta in SNIIP combined with high pulsar velocities is thus a strong argument that the explosion of core-collapse supernovae is accompanied by the violation of the point symmetry.

At present the likely mechanism for the asymmetry in core-collapse supernovae is the large-scale neutrino convection (Herant et al. 1992; Scheck et al. 2004), although the ejection of the supernova envelope with the required kinetic energy of  $\sim 10^{51}$  erg remains problematic (Buras et al. 2003).

The detection of the bipolar structure of the <sup>56</sup>Ni ejecta in normal SNIIP raises another intriguing question, whether the bipolar structure could emerge in the neutrino-driven explosion mechanism? This problem was recently discussed in connection with the interpretation of the bipolar ejecta of Cas A and SN1987A (Burrows et al. 2005). Authors considered the role of the moderate rotation in the creation of jets within neutrino-driven mechanism. However, it should be emphasised, that both these supernovae might in principle originate from presupernovae with the relatively fast rotation: Cas A is SNIb/c, and the nebular ring around SN1987A indicates fast rotation too. As to SN2004dj and SN1999em, which are normal SNIIP, here we deal with cores of red supergiants that are presumably slow rotators. Therefore, it might be well that the origin of the asymmetric bipolar <sup>56</sup>Ni ejection in SNIIP has nothing to do with the rotation.

We are grateful to V.L. Afanasiev, N.B. Borisov nad S.S. Kaisin for the help in observations. The work is partially supported by RFBR grants 4-02-17255, 03-02-16341 and 04-2-16349.

## REFERENCES

Ardeljan N.V., Bisnovatyi-Kogan G.S. and Moiseenko S.G., Mon. Not. R. astron. Soc. **359**, 333 (2005)

Afanasiev V.L. and Moiseev A.V., Astron. Lett. 31, 194 (2005)

Blinnikov S.I., Imshennik V.S., Nadezhin D.K., Novikov I.D., Perevodchikova T.V. and Polnarev A.G., Sov. Astron. 34, 595 (1990)

Buras R., Rampp M., Janka H.-Th. and Kifonidis K., Phys. Rev. Lett. 90, 1101 (2003)

Burrows A., Walder R., Ott C.D. and Livne E., *The fate of the most massive stars. ASP Conf. Ser. V. 332*, Ed. R. Humphreys, K. Stanek (ASP, San Francisco, 2005), p.358

Catchpole R. M., Menzies J. W., Monk A. S. et al., Mon. Not. R. astr. Soc. 229, 15P (1987)

Catchpole R. M., Whitelock P. A., Feast M. W. et al., Mon. Not. R. astr. Soc. 231, 75P (1988)

Chugai N.N. Sov. Atron. Lett. 13, 282 (1987)

Chugai N.N., Astron. Tsirk. 1525, 15, (1988)

Chugai N.N., Sov. Astron. **35**, 171 (1991)

Chugai N.N., Astrophys. J. 428, L17 (1994)

Colgate S.A. and White R.H., Astrophys. J. **143**, 626 (1966)

Elmhamdi A., Danziger I.J., Chugai N.N. et al. Mon. Not. R. astr. Soc. 338, 939 (2003)

Elmhamdi A., Chugai N.N. and Danziger I.J., Astron. Astrophys. 404, 1077 (2003)

Fransson C. and Chevalier R.A., Astrophys. J. 343, 323 (1989)

Freedman W.L., Madore B.F., Gibson B.K. et al., Astrophys. J. 553, 47 (2001)

Grasberg E.K., Imshennik V.S. and Nadyozhin D.K., Astroph. Space Sci. 10, 28 (1971)

Herant M., Benz W. and Colgate S. Astrophys. J. 395, 642 (1992)

Hobbs G., Lorimer D.R., Lyne A.G., and Kramer M. Mon. Not. R. astr. Soc. 360, 974 (2005)

Korcakova D., Mikulasek Z., Kawka A. et al., Int. Bull. Var. Stars 5605, 1 (2005)

Leonard D.C., Filippenko A.V., Li W. et al, Astron. J. 124, 2490 (2002)

Li H. and McCray R., Astrophys. J. **405**, 730 (1993)

Liu W. and Dalgarno A., Astrophys. J. **454**, 472 (1995)

Nadyozhin D.K, Mon. Not. R. astr. Soc. **346**, 97 (2003)

Nakano S., Itegaki K., Bouma R.J., Lehky M. and Hornoch K., IAU Circ. 8377, 1 (2004)

Phillips M.M. and Williams R.E., *Supernovae*, Ed. S. E. Woosley (Springer, N.Y., 1991), p.36

Scheck L., Plewa T., Janka H.-Th., Kifonidis K. and Müller E., Phys. Rev. Lett. **92**, 1103 (2004)

Schlegel D., Finkbeiner D. and Davis M., Astrophys. J. 500, 525 (1998)

Seaton M.J., Mon. Not. R. astr. Soc. 187, 75P (1979)

Suntzeff N.B. and Bouchet P.), Supernovae, Ed. S. E. Woosley (Springer, N.Y., 1991), p.3

Spyromilio J. and Pinto P.A., SN1987A and other supernovae, Ed. I.J. Danziger and K. Kjär (ESO, Garching,1991), p.423

Utrobin V.P., Astron. Lett. **30**, 3293 (2004)

Wang L., Wheeler J.C. and Höflich P., Astrophys. J. 579, 671 (2002)

Wang X., Yang Y., Zhang T., Ma .J, Zhou X., Li W., Lou Y.-Q. and Li Z.), Astrophys. J. **626**, L89 (2005)

Weaver T.A. and Woosley S.E. in *Ann. NY Acad. Sci. Ninth Texas Symp. on Relativistic Astrophysics*, Ed. J. Ehlers, J. Perry and M. Walker (N.Y. Acad. Sci., N.Y.,1980), p.335

Woosley S.E. and Weaver T.A., Astrophys. J. Suppl. 101, 181 (1995)

Zickgraf F.-J., Humphreys R.M., Sitko M.L. and Manley T., Publ. Astron. Soc Pacific **102**, 925 (1990)

Xu Y. and McCray R., Supernovae, Ed. S. E. Woosley (Springer, N.Y., 1991), p.444

This preprint was prepared with the AAS IATEX macros v5.2.

Table 1: SN2004dj photometric data

JD2450000+	В	V	Rc	CCD
1929.4831	18.337	17.836	17.434	K
3321.6191	15.949	14.727	14.110	$\mathbf{E}$
3355.5434	16.100	15.068	14.210	VA
3357.5453	16.140	15.082	14.210	VA
3358.5417	16.116	15.083	14.187	VA
3361.5745	16.128	15.129	14.243	VA
3385.3628	16.320	15.342	14.311	$\mathbf{E}$
3386.3845	16.346	15.345	14.326	$\mathbf{E}$
3387.4160	16.320	15.351	14.320	$\mathbf{E}$
3436.4913	16.534	15.666	14.662	$\mathbf{E}$
3437.2683	16.539	15.689	14.678	$\mathbf{E}$
3500.4002	16.044			Е

Table 2: Log of spectral observations

Date	JD2450000+	Spectrograph	Range	Resolution
			Å	Å
18.10.04	3298.5	LAT Scorpio	3700 - 7500	13
22.10.04	3301.5	1-m UAGS	4000 - 7800	7.6
09.11.04	3320.3	LAT Scorpio	3900 - 7500	13
15.11.04	3325.3	LAT MPFS	4000 - 7000	6
16.01.05	3387.2	LAT MPFS	4000 - 7000	6
05.02.05	3406.8	LAT Scorpio	3900 - 7500	13
09.05.05	3500.3	LAT Scorpio	5700 - 7400	6
07.06.05	3529.4	LAT Scorpio	4000 - 5700	6

Table 3: Flux and luminosity of  ${\rm H}\alpha$ 

Date	t	F	$F^{\mathrm{corr}}$	L
	days	${ m erg~s}^{-1}$	$1 \text{ cm}^{-2}$	${ m erg~s^{-1}}$
18.10.04	127	$2.37 \times 10^{-12}$	$2.72 \times 10^{-12}$	$3.19 \times 10^{39}$
09.11.04	149	$1.82 \times 10^{-12}$	$2.09 \times 10^{-12}$	$2.45\times10^{39}$
15.11.04	155	$1.84 \times 10^{-12}$	$2.12 \times 10^{-12}$	$2.49 \times 10^{39}$
16.01.05	217	$2.27 \times 10^{-12}$	$2.61 \times 10^{-12}$	$3.07\times10^{39}$

Table 4: Parameters of components of lines of  $[O\,I]$  and  $[Ca\,II]$  doublets

Doublet	Age	Component	$v_{ m r}$	$\overline{w}$	A	R
	days		$\mathrm{km}$	$s^{-1}$		
[O I]	237	1	-1380	730	1.55	1.33
[OI]	237	2	-30	750	1.21	1.33
[OI]	330	1	-1200	750	1.2	1.8
[OI]	330	2	60	750	1.9	1.8
[CaII]	149	1	-1500	440	9.5	1.1
[CaII]	149	2	200	1300	0.53	1.1
[CaII]	237	1	-1270	470	8.8	1.3
[Ca II]	237	2	200	1300	1.3	1.3

Table 5: Parameters of  $^{56}\mathrm{Ni}$  distribution

$\theta$	$v_{\rm s}$	$v_1$	$v_2$	$M_1/M_{ m s}$	$M_2/M_{ m s}$	$M_{\rm c}$
		${\rm km~s^{-1}}$				$M_{\odot}$
30°	1400	2700	3500	1.07	0.49	1.3

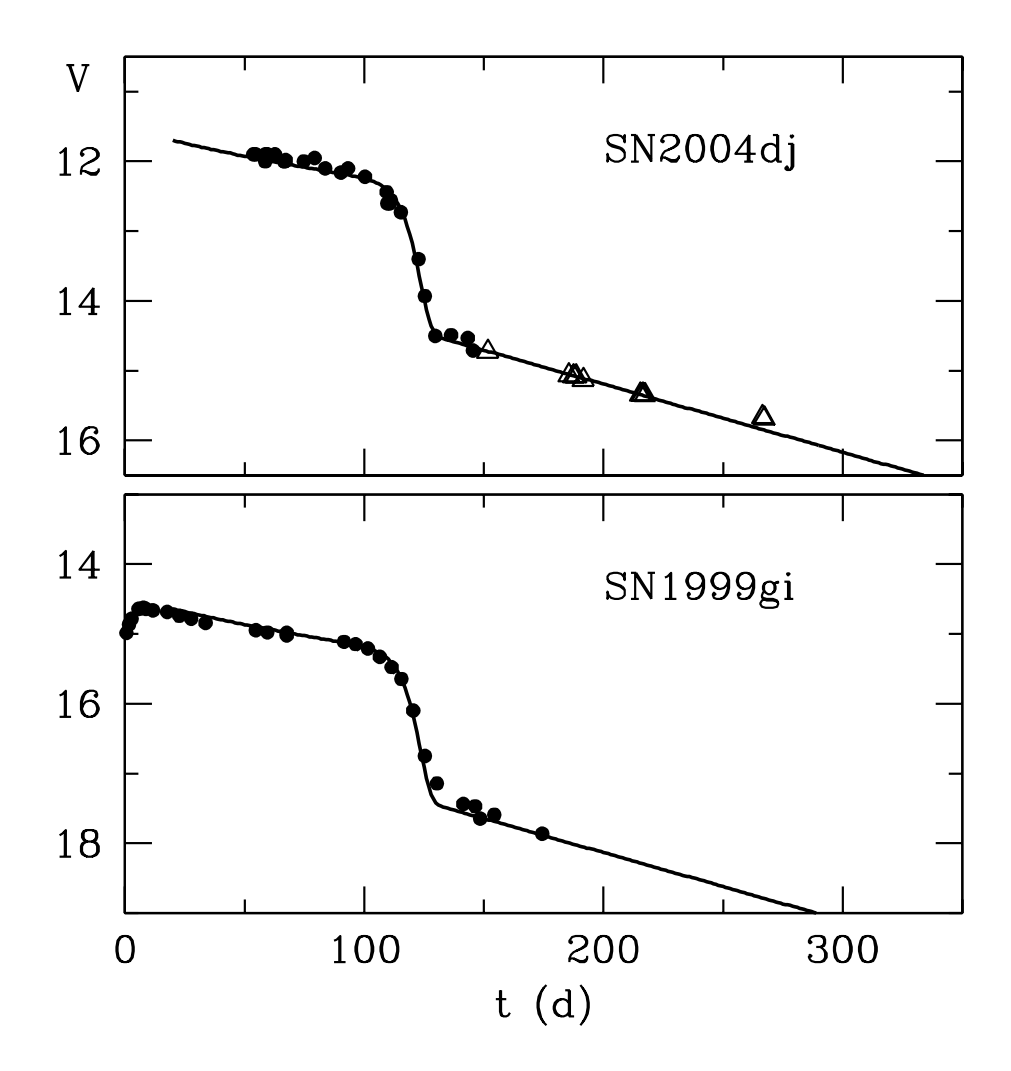


Fig. 1.— Light curves in V band of SN2004dj and SN1999gi. *Triangles* are our data, *points* are amateurs data. Solid line shows the analytical fit, the same in both cases. The time is counted from the adopted explosion moment (2004 June 13).

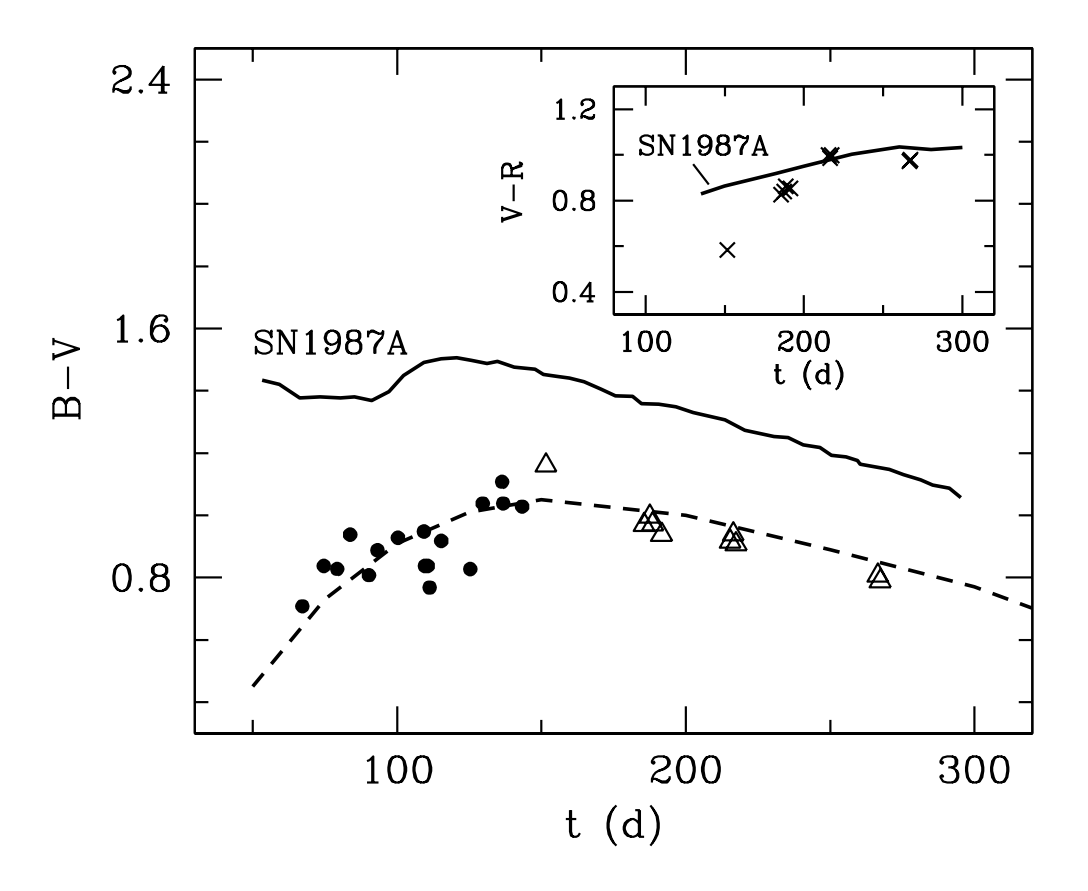


Fig. 2.— Color B-V of SN2004dj. Triangles are our data, points are amateurs data. Solid line is the SN1987A color, dashed line is the lower envelope of B-V colors of SNIIP (Elmhamdi et al. 2003b). Inset shows the V-R color of SN2004dj (crosses) in comparison with the color of SN1987A (line).

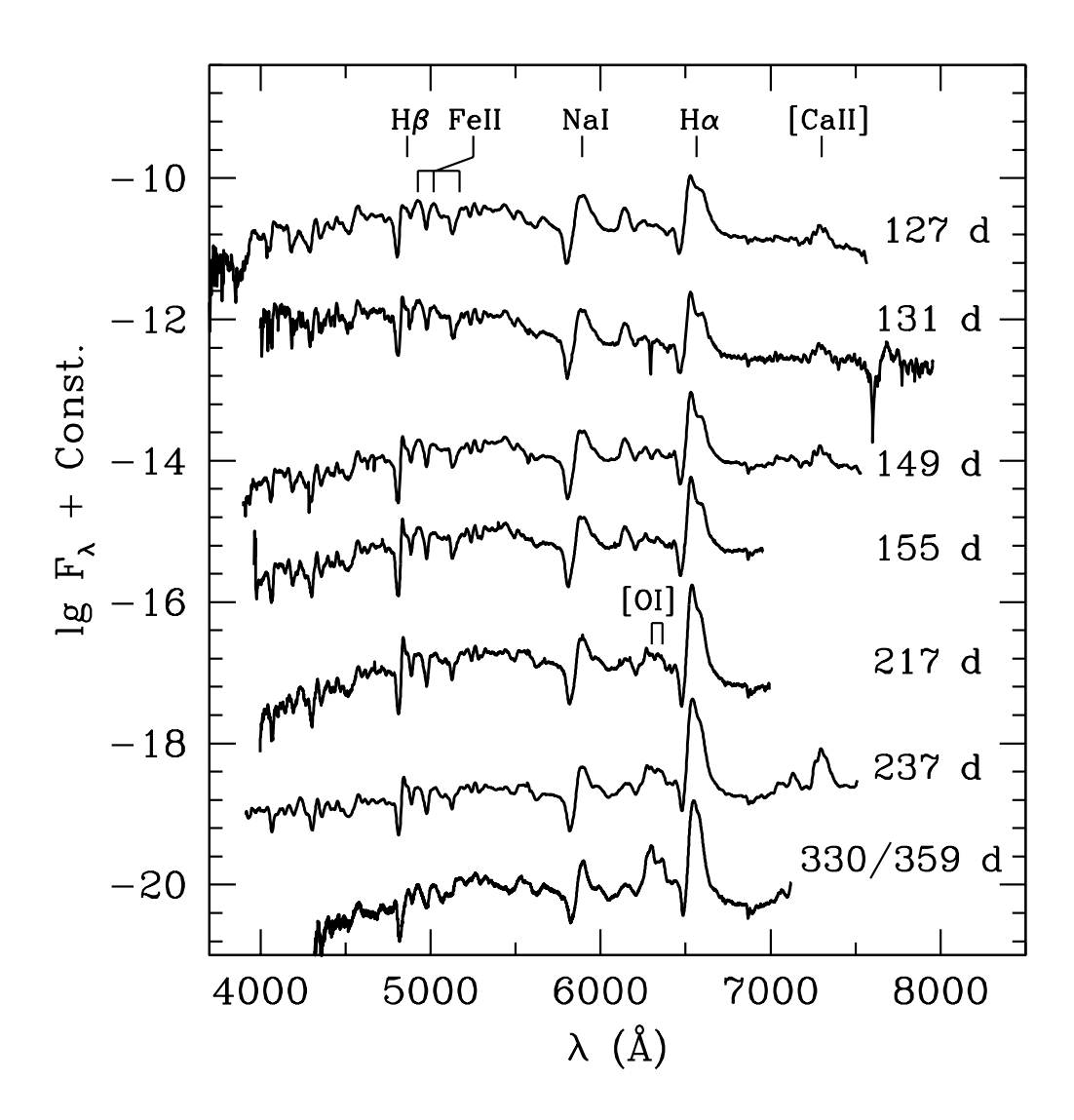


Fig. 3.— Spectra of SN2004dj at different age and major identifications. The wavelenth is corrected for the galaxy redshift. The age next to spectrum is measured from the explosion (2004 June 13).

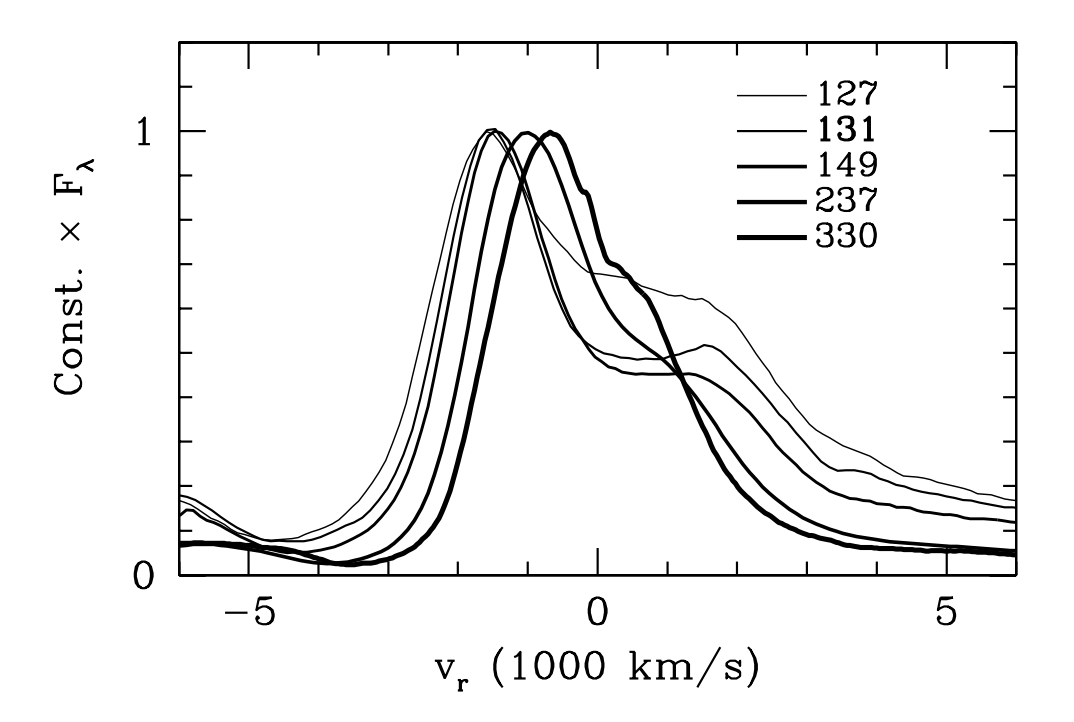


Fig. 4.— Evolution of  $H\alpha$  in spectra of SN2004dj. The age is indicated next to line of a corresponding width.

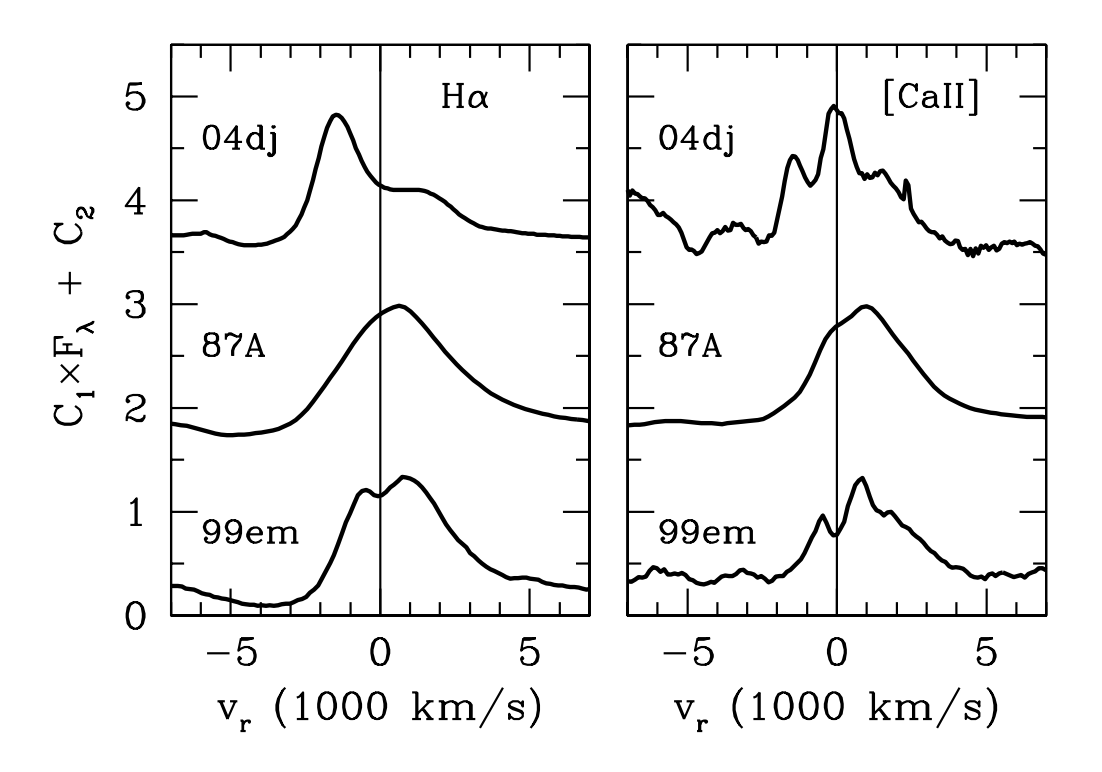


Fig. 5.—  ${\rm H}\alpha$  line and [Ca II] doublet in spectrum of SN2004dj on day 149, in spectrum of SN1987A on day 198 and in spectrum of SN1999em on day 140. The radial velocity of [Ca II] is given for the line of 7291 Å.

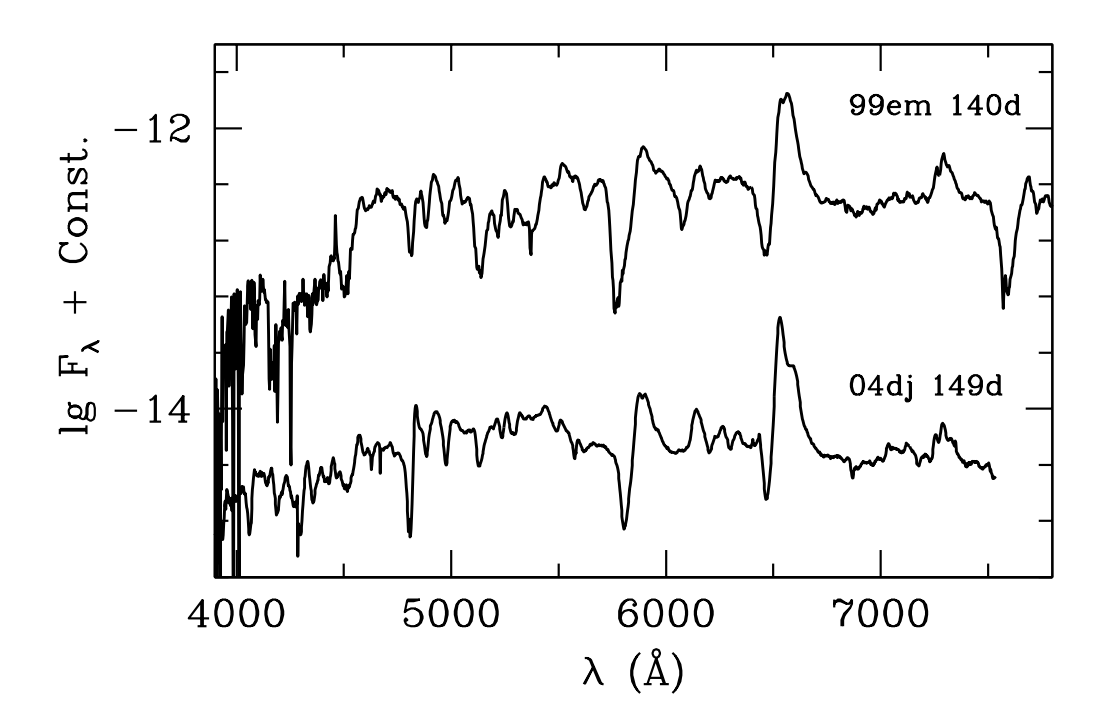


Fig. 6.— Spectra of SN2004dj and SN1999em at similar phases. Note, the difference of profiles and quasicontinua around 5600  $\hbox{Å}.$ 

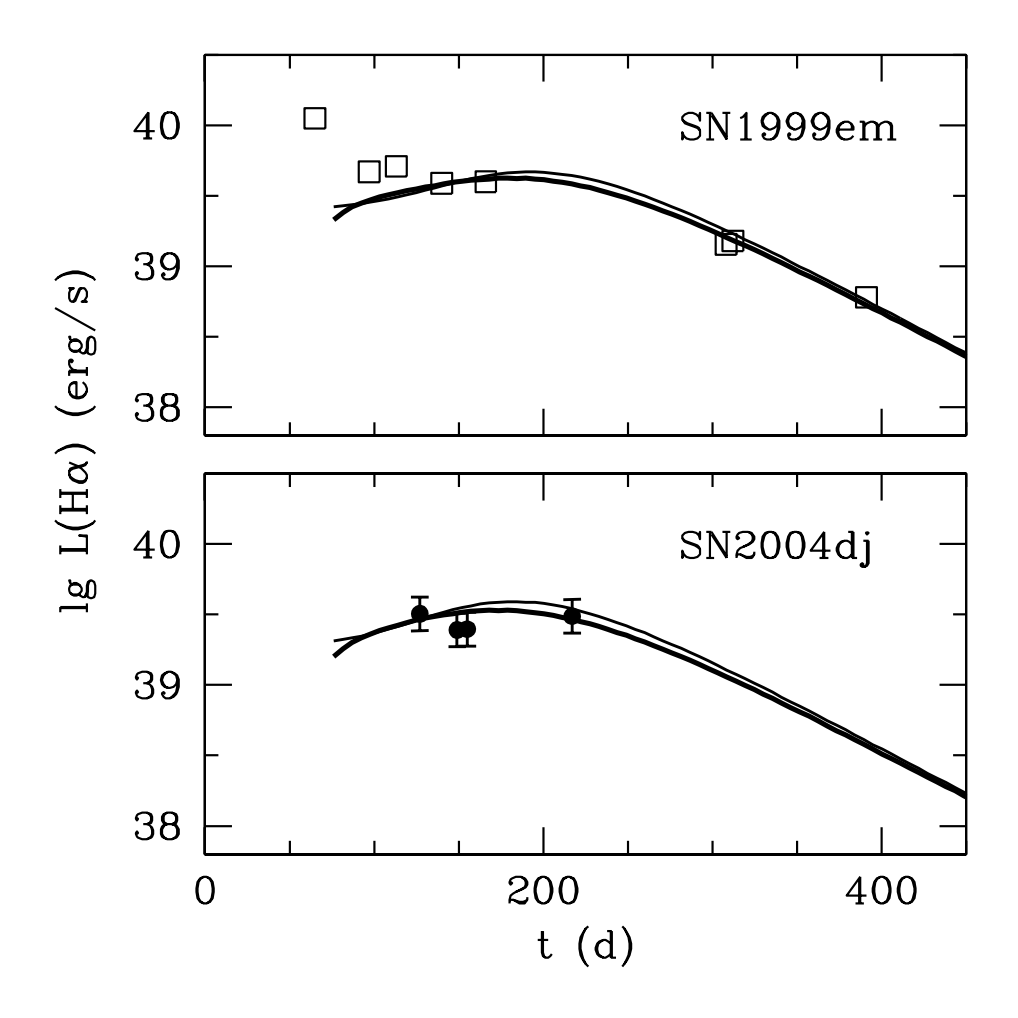


Fig. 7.— Evolution models of H $\alpha$  for SN1999em and SN2004dj. Data for SN1999em (upper panel, squares) are taken from Elmhamdi (2003b). Model of SN1999em suggests  $^{56}$ Ni mass of 0.027  $M_{\odot}$  and two options of mixing parameter  $f_{\rm s}=2$  (thick line) and  $f_{\rm s}=20$  (thin line). For SN2004dj the model is the same as for SN1999em, but  $^{56}$ Ni mass is 0.02  $M_{\odot}$ .

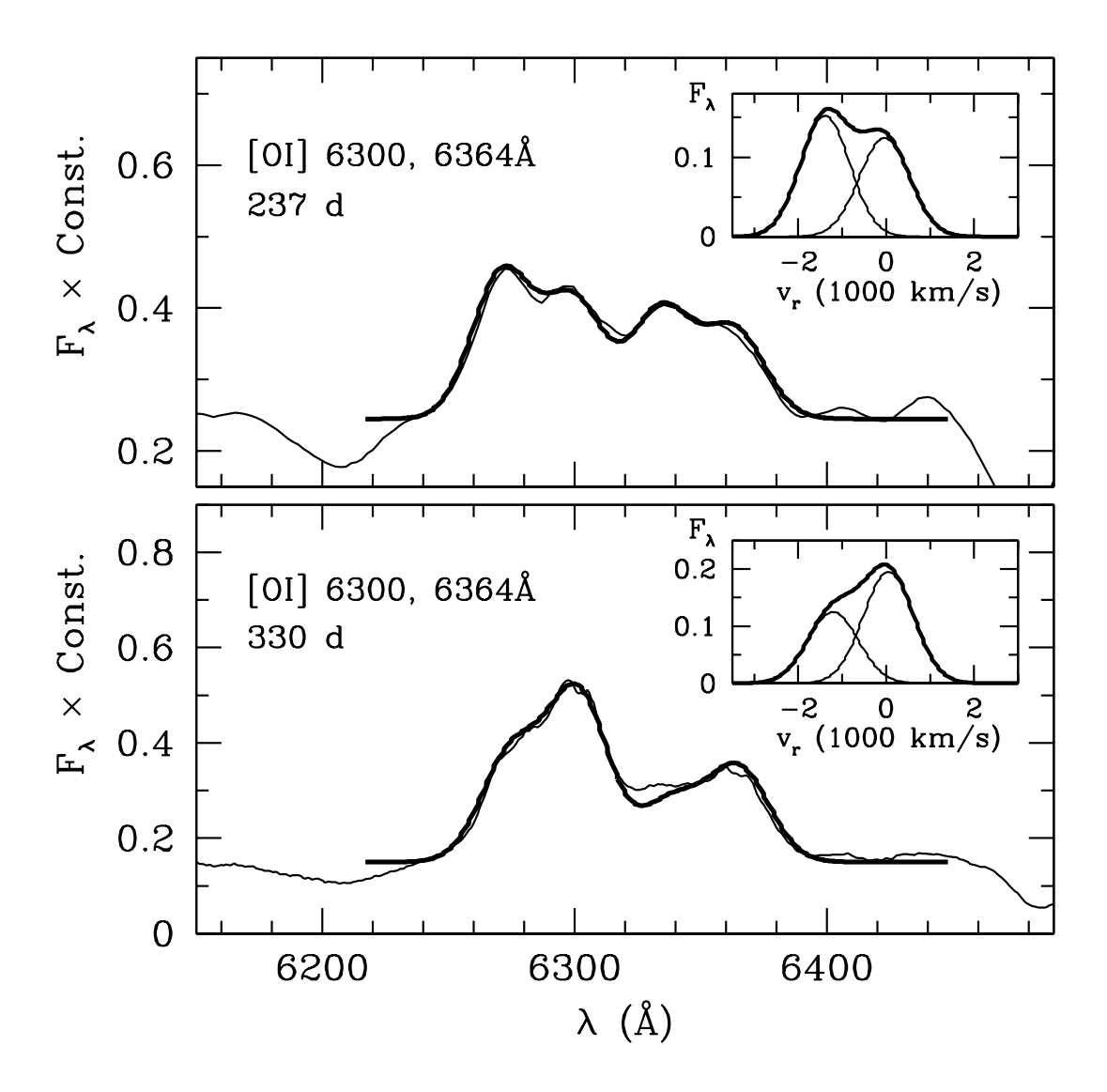


Fig. 8.— Reconstruction of the line profile of [O I] 6300, 6364 Å doublet in SN2004dj on day 237 and 330. *Thick* line is the model, *thin* line is observation. Inset shows model line profile (*thick* line) along with gaussian components.

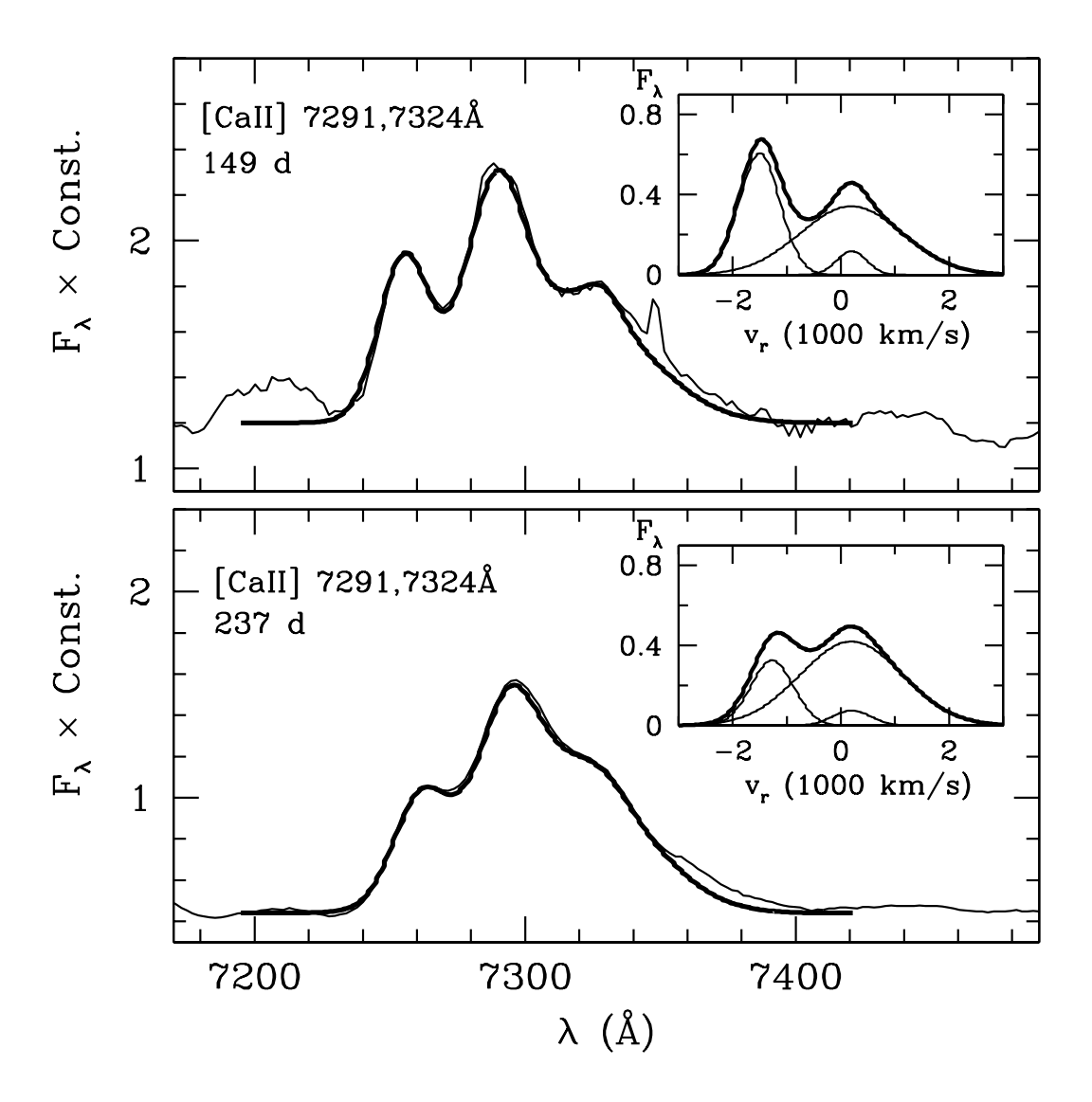


Fig. 9.— Reconstruction of the line profile of [Ca II] 7291, 7324 Å doublet in SN2004dj on day 149 and 237. *Thick* line is the model, *thin* line is observation. Inset shows model line profile (*thick* line) along with gaussian components.

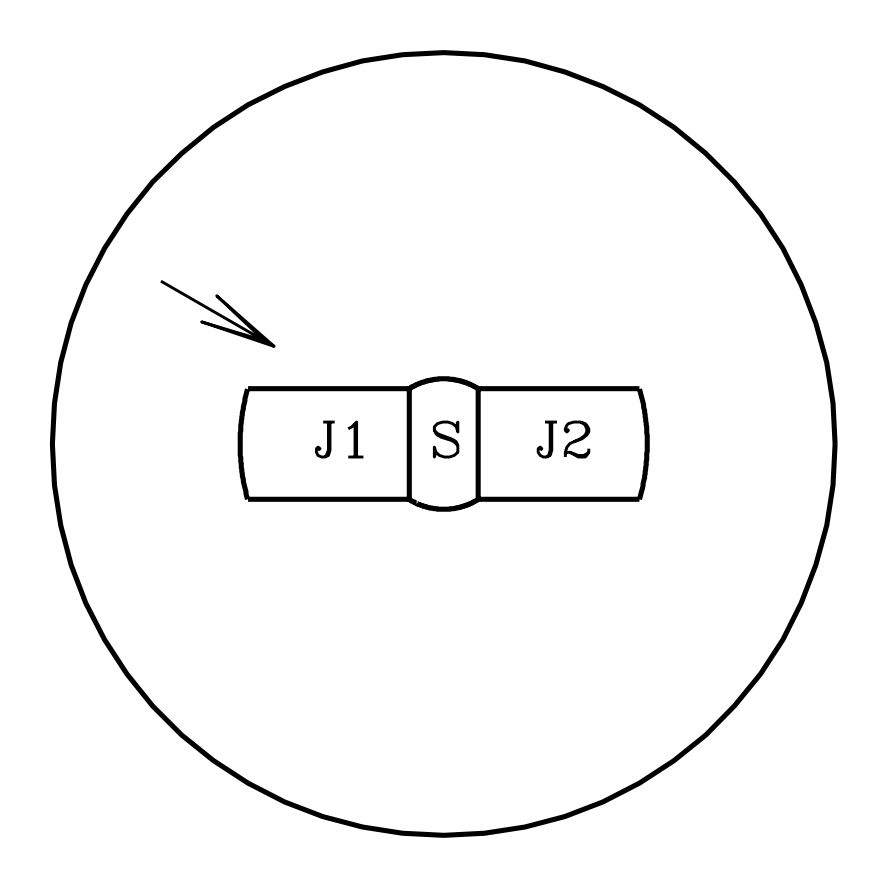


Fig. 10.— Schematic representation of the spherical envelope of SN2004dj with bipolar  $^{56}$ Ni distribution, The  $^{56}$ Ni distribution includes the central component S and two jets J1 and J2. Arrow shows the line of sight.

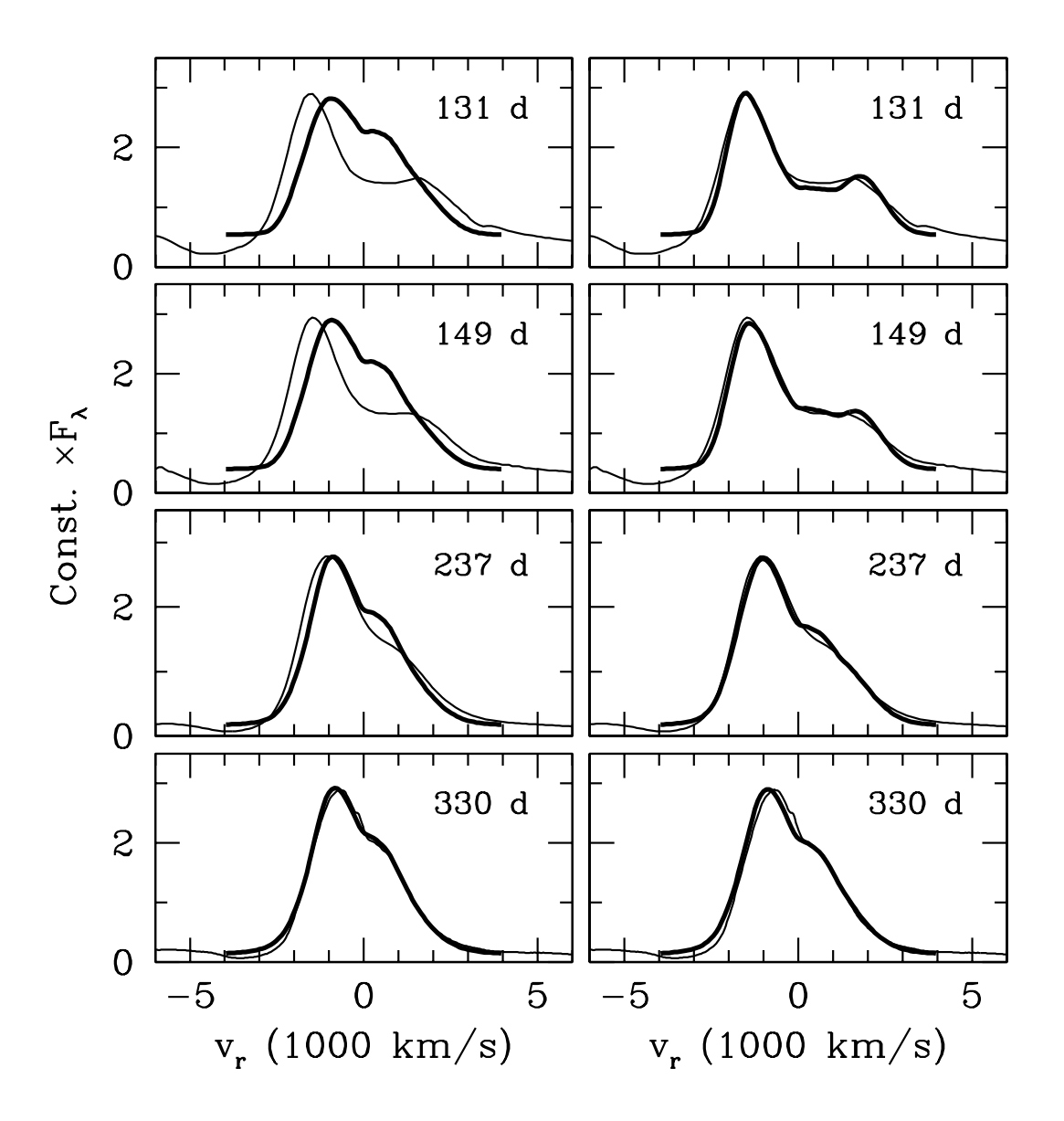


Fig. 11.— Models of the H $\alpha$  in SN2004dj with the asymmetric bipolar <sup>56</sup>Ni distribution. Thick line is the model, thin line is observations. Models of <sup>56</sup>Ni distribution without cocoon (*left* panels) and with cocoon (*right* panels) are shown.

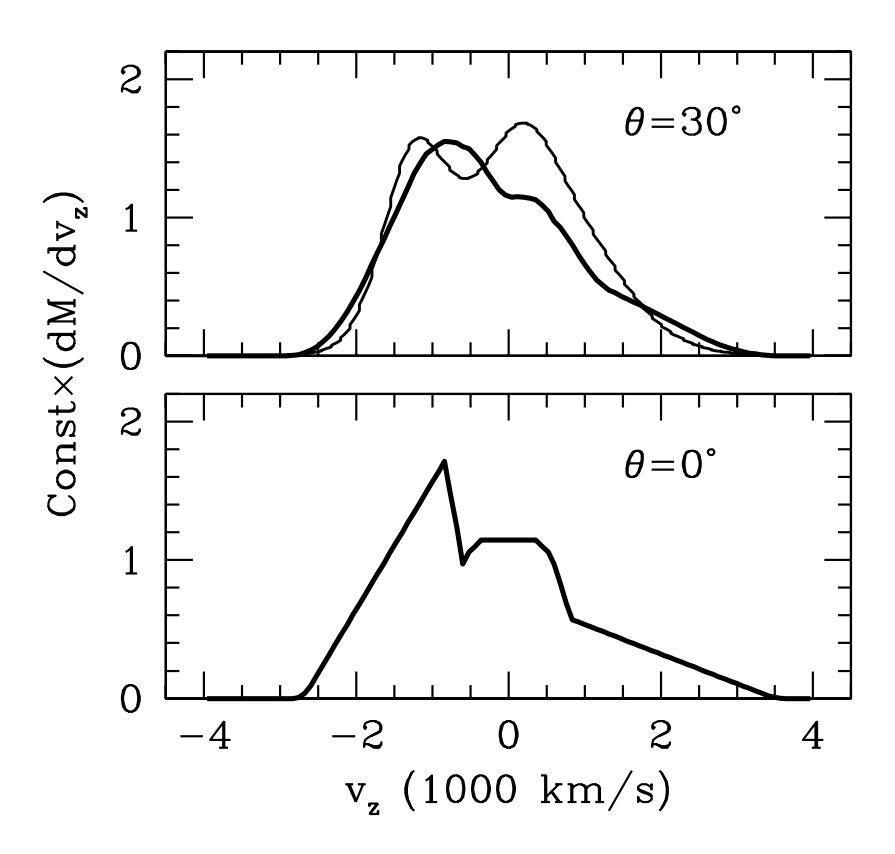


Fig. 12.— Mass distribution of  $^{56}$ Ni along the radial velocity. Upper panel shows projection on the line of sight (*thick* line) together with the model profile of [Ca II] 7291 Å line on day 149 (Fig. 9). The lower panel shows the projection of  $^{56}$ Ni distribution on the polar axis of ejecta.